

A unified theory of spin and charge excitations in high- T_c cuprates: Quantitative comparison with experiment and interpretation

Maciej Fidrysiak^{1,*} and Józef Spałek^{1,†}

¹*Institute of Theoretical Physics, Jagiellonian University, ul. Łojasiewicza 11, 30-348 Kraków, Poland*

We provide a unified interpretation of both paramagnon and plasmon modes in high- T_c copper-oxides, and verify it quantitatively against available resonant inelastic x -ray scattering (RIXS) data across the hole-doped phase diagram. Three-dimensional extended Hubbard model, with included long-range Coulomb interactions and doping-independent microscopic parameters for both classes of quantum fluctuations, is used. Collective modes are studied using VWF+ $1/\mathcal{N}_f$ approach which extends variational wave function (VWF) scheme by means of an expansion in inverse number of fermionic flavors ($1/\mathcal{N}_f$). We show that intense paramagnons persist along the anti-nodal line from the underdoped to overdoped regime and undergo rapid overdamping in the nodal direction. Plasmons exhibit a three-dimensional character, with minimal energy corresponding to anti-phase oscillations on neighboring CuO_2 planes. The theoretical spin- and charge excitation energies reproduce semi-quantitatively RIXS data for $(\text{Bi, Pb})_2(\text{Sr, La})_2\text{CuO}_{6+\delta}$. The present VWF+ $1/\mathcal{N}_f$ analysis of dynamics and former VWF results for static quantities combine into a consistent description of the principal properties of hole-doped high- T_c cuprates as strongly correlated systems.

Introduction—A profound problem in condensed matter physics is to unveil the microscopic structure of both the single- and many-particle excitations in high-temperature (high- T_c) cuprate superconductors (SC) as they evolve from antiferromagnetic (AF) insulator, through the SC phase, to a Fermi-Liquid normal state [1]. At low doping, localized holes coexist with collective spin-wave excitations which are now well understood within the framework of Heisenberg-type models [2, 3]. Much less is known about the microscopic mechanism governing single- and many-particle excitations at moderate and high doping levels, where no AF or charge order occur. Itinerant carriers are expected to cause Landau overdamping of spin-wave modes, particularly after AF order has been suppressed. On the contrary, resonant inelastic x -ray scattering (RIXS) and inelastic neutron scattering experiments demonstrate that robust *paramagnons* persist across whole hole-doping phase diagram [4–19]. In addition, RIXS provides evidence for low-energy charge modes (*acoustic plasmons*) in both hole- and electron-doped cuprates [20–25]. Over the years, several distinct high- T_c SC mechanisms, based either on fluctuations (magnetic [17, 26, 27] and charge [28, 29]), or local correlations [30], have been proposed. In effect, a unified quantitative theory of the equilibrium thermodynamic properties, as well as correlated single-particle and collective excitations in high- T_c copper-oxides, is now in demand to single-out the microscopic SC pairing scenario.

The current theoretical frameworks, used interpret RIXS data for copper-oxides, encompass determinant quantum Monte-Carlo (DQMC) [19], Hubbard-operator large- N limit [31–33], random-phase-approximation (RPA) [7], and spin-wave theory (SWT) [3, 10]. Those have been successful in explaining certain aspects of experiments, yet none of them provides a unified description of both spin and charge excitations within a single

microscopic model with fixed parameters. Specifically, DQMC yields well controlled imaginary-time susceptibilities, but suffers from the sign problem and requires analytic continuation of numerical data, which reduces its reliability in regard to dynamics. Moreover, due to lattice-size limitations, DQMC cannot account for long-range Coulomb repulsion that is considered essential for plasmon physics in high- T_c materials [34]. On the other hand, Hubbard-operator large- N limit with long-range interactions included, reproduces measured plasmon spectra [25], but it is intended for the strong-coupling situation (t - J / t - J - V models) and seems to overestimate correlation effects, such as bandwidth renormalization. This has been compensated by adopting bare nearest-neighbor hopping scale $|t| \approx 0.5$ - 0.75 eV [25, 33, 35], larger than accepted values $|t| \approx 0.3$ - 0.4 eV. Also, the Hubbard-operator $1/N$ expansion does not treat the collective modes on the same footing and privileges charge- over spin excitations [36, 37]. On the other hand, the RPA approach requires adopting unphysically small on-site repulsion $U \sim 1.5|t|$ [7, 38]. Finally, accurate fits to the paramagnon spectra are obtained by applying SWT to extended Heisenberg models, including both cyclic- and long-range exchange [3, 10]. Yet, SWT disregards charge excitations, and the underlying large-spin approximation yields magnetic order at high-doping, in disagreement with experiment. In effect, a consistent theoretical picture of spin- and charge dynamics in metallic high- T_c cuprates has not been reached so far.

We fill-in this gap and reconcile quantitatively both paramagnon and plasmon excitations in hole-doped cuprates within a single microscopic model with realistic and doping-independent microscopic parameters. We start from a three-dimensional Hubbard Hamiltonian, with long-range Coulomb repulsion included, and analyze it using recently developed VWF+ $1/\mathcal{N}_f$ scheme [39, 40] that combines Variational Wave Function (VWF) ap-

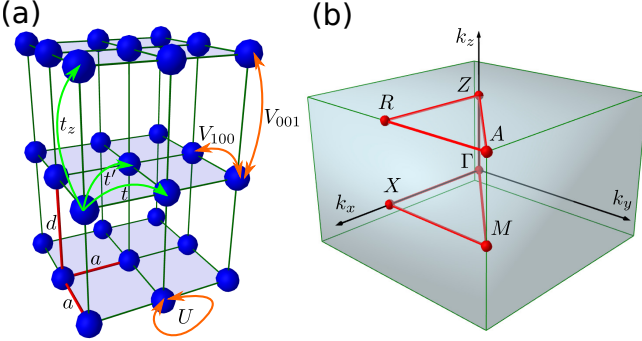


FIG. 1. (a) Layered square lattice with in-plane lattice constant a and interlayer spacing d . Model parameters are marked inside: green and orange arrows indicate hopping integrals and interactions, respectively. Only two out of infinite number of long-range Coulomb integrals, V , are shown. (b) First Brillouin zone with marked Γ -X-M- Γ -Z-R-A-Z contour.

proach with expansion in inverse number of fermionic flavors ($1/\mathcal{N}_f$). This allows us to account for both spin- and charge quantum fluctuations around the correlated ground state *on the same footing*, which is needed for an unbiased analysis. Explicitly, we show that intense and propagating paramagnons persist in the metallic phase along the anti-nodal (Γ -X) Brillouin-zone (BZ) direction in wide doping range, but become rapidly overdamped along the nodal (Γ -M) line. This reflects the experimental trends for multiple copper-oxide families [4–19]. Also, plasmons are shown to exhibit a substantial three-dimensional character. The results agree semi-quantitatively with available RIXS data for $(\text{Bi, Pb})_2(\text{Sr, La})_2\text{CuO}_{6+\delta}$. In effect, VWF+ $1/\mathcal{N}_f$ emerges as a platform for quantitative interpretation of spectroscopic data for strongly correlated materials, and combines with former equilibrium VWF results [30, 41–45] into a consistent overall description of high- T_c cuprate superconductors.

Model and method—We employ extended Hubbard model Hamiltonian

$$\hat{\mathcal{H}} = \sum_{ij\sigma} t_{ij} \hat{c}_{i\sigma}^\dagger \hat{c}_{j\sigma} + U \sum_i \hat{n}_{i\uparrow} \hat{n}_{i\downarrow} + \frac{1}{2} \sum_{i \neq j} V_{ij} \hat{n}_i \hat{n}_j, \quad (1)$$

where $\hat{c}_{i\sigma}^\dagger$ ($\hat{c}_{i\sigma}$) are creation (annihilation) operators on site i for spin σ , $\hat{n}_{i\sigma} \equiv \hat{c}_{i\sigma}^\dagger \hat{c}_{i\sigma}$, and $\hat{n} \equiv \hat{n}_\downarrow + \hat{n}_\uparrow$. The model is defined on a stacked two-dimensional square lattice ($200 \times 200 \times 16$ sites) with in-plane spacing a , and interlayer distance d (cf. Fig. 1). We adopt standard values of in-plane nearest-neighbor (n.n.) and next-nearest hopping integrals, $t = -0.35$ eV and $t' = 0.25|t|$, respectively, and small out-of-plane one $t_z = -0.01|t|$, reflecting substantial interlayer distance in Bi2201. The on-site Coulomb repulsion is set to $U = 6|t|$, which is backed by recent estimates of effective $U \sim 6$ -9 $|t|$ [46], and has been adopted in a single-layer model study [39]. The last term

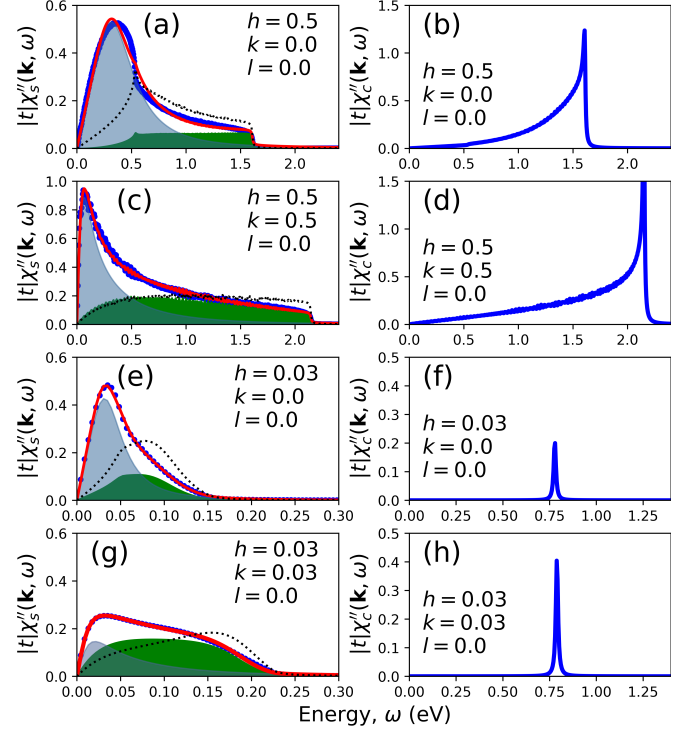


FIG. 2. Representative $\text{SGA}_f + 1/\mathcal{N}_f$ results for $\delta = 0.16$. Blue points and lines are the calculated imaginary parts of spin [(a), (c), (e), (g)] and charge [(b), (d), (f), (h)] dynamical susceptibilities for wave vectors detailed inside the panels. On the left, the green-shaded areas represent incoherent contribution, whereas blue-shaded area is the harmonic oscillator peak [cf. Eq. (3)]. The red line is the sum of the two, and black dotted lines represent Lindhard response. Note emergence of the coherent plasmon peaks close to the BZ center.

accounts for long-range Coulomb repulsion. At large distances, V_{ij} may be obtained as a solution of a discretized Laplace equation [47], yielding in \mathbf{k} -space

$$V_{\mathbf{k}} = \frac{V_c}{\gamma \Phi(k_x, k_y) + 1 - \cos(k_z d)}, \quad (2)$$

where $\Phi(k_x, k_y) \equiv 2 - \cos(k_x a) - \cos(k_y a)$, $V_c = e^2 d / (2a^2 \epsilon_\perp \epsilon_0)$, $\gamma = \epsilon_\parallel d^2 / (\epsilon_\perp a^2)$, and ϵ_\parallel (ϵ_\perp) are in-plane (out-of-plane) dielectric constants. We select $\gamma = 10$ and $V_c = 46|t|$, which assumes a dominant lattice-anisotropy effect on γ (see [25]) and yields $\epsilon_\perp \approx 4.66$, comparable with the high-energy values $\epsilon_\perp \approx 4$ -4.5 reported for Bi2201 [48]. Also, the resulting n.n. repulsion $V/|t| \approx 2.03$ is consistent with *ab initio* [49] estimates for related materials (2.36 for $\text{HgBa}_2\text{CuO}_4$ and 2.30 for La_2CuO_4). Note that the plasmon gap can be estimated as $\Delta_p^2 = 2\hbar^2 V_c n_c / (m^* a^2 \gamma)$, with m^* and n_c being the correlation-renormalized carrier mass and concentration, respectively. The scale of Δ_p is thus sensitive to $V_c/\gamma = 4.6|t|$. Hereafter we set the temperature to $k_B T = 0.4|t|$ to stay clear of broken-symmetry [50] states.

The model (1) is solved using VWF+1/ \mathcal{N}_f scheme which has been elaborated extensively in a methodological paper [40], regarded here as a Supplemental Material. In brief, the method is based on the energy functional $E_{\text{var}} \equiv \langle \Psi_{\text{var}} | \hat{\mathcal{H}} | \Psi_{\text{var}} \rangle / \langle \Psi_{\text{var}} | \Psi_{\text{var}} \rangle$, defined in terms of the variational state $|\Psi_{\text{var}}\rangle \equiv \hat{P}_{\text{var}}(\boldsymbol{\lambda})|\Psi_0\rangle$, where $|\Psi_0\rangle$ is an uncorrelated wave function. The operator $\hat{P}_{\text{var}}(\boldsymbol{\lambda})$ adjusts weights of many-body configurations in $|\Psi_{\text{var}}\rangle$ and depends on a vector composed of variational parameters, $\boldsymbol{\lambda}$, subjected to additional constraints [40]. By application of linked-cluster expansion in real space, $E_{\text{var}} = E_{\text{var}}(\mathbf{P}, \boldsymbol{\lambda})$ becomes a functional of “lines”, $P_{i\sigma j\sigma'} \equiv \langle \hat{c}_{i\sigma}^\dagger \hat{c}_{j\sigma'} \rangle$, and $\boldsymbol{\lambda}$. We use Statistically-consistent Gutzwiller Approximation (SGA)[51] to truncate diagrammatic series for E_{var} , which results in SGA $_f$ +1/ \mathcal{N}_f variant of VWF+1/ \mathcal{N}_f . We also approximate long-range part of Coulomb energy as $\langle \hat{V} \rangle \approx \frac{1}{2} \sum_{i \neq j} V_{ij} \langle n_i \rangle \langle n_j \rangle$, effectively disregarding non-local lines which is justified at large distances. As a second step, $\mathbf{P} \rightarrow \mathbf{P}(\tau)$ and $\boldsymbol{\lambda} \rightarrow \boldsymbol{\lambda}(\tau)$ are promoted to (imaginary-time) dynamical fields. Finally, the Euclidean action for $\mathbf{P}(\tau)$, $\boldsymbol{\lambda}(\tau)$, and other auxiliary fields, is constructed and used to generate dynamical spin- and charge- collective susceptibilities, $\chi_s(\mathbf{k}, i\omega_n)$ and $\chi_c(\mathbf{k}, i\omega_n)$, respectively. Analytic continuation is carried out as $i\omega_n \rightarrow \omega + i0.02|t|$.

To make a comparison with experiment, it is necessary to extract paramagnon energies and their damping rates from the calculated spectra. This is done by damped harmonic oscillator modeling [52] of the imaginary part of the dynamical spin susceptibility

$$\chi_s''(\mathbf{k}, \omega) = \frac{2A(\mathbf{k})\gamma(\mathbf{k})\omega}{[\omega^2 - \omega_0^2(\mathbf{k})]^2 + 4\gamma^2(\mathbf{k})\omega^2} + \chi_{s,\text{in}}''(\mathbf{k}, \omega), \quad (3)$$

where $A(\mathbf{k})$, $\omega_0(\mathbf{k})$, and $\gamma(\mathbf{k})$ denote the amplitude, bare energy, and damping rate, respectively. Crucially, $\omega_0(\mathbf{k})$ *does not* represent the physical paramagnon energy, and it remains non-zero even if magnetic excitations are *overdamped*. The relevant parameter is thus the real part of the quasiparticle pole, $\omega_p(\mathbf{k}) = \sqrt{\omega_0^2(\mathbf{k}) - \gamma^2(\mathbf{k})}$ if $\omega_0(\mathbf{k}) > \gamma(\mathbf{k})$, and zero otherwise. The last term represents the incoherent part, $\chi_{s,\text{in}}''(\mathbf{k}, \omega)$, providing background to the oscillator peak. We model $\chi_{s,\text{in}}''(\mathbf{k}, \omega)$ as the Lindhard susceptibility (defined as the loop integral, evaluated with Landau quasiparticle Green’s functions), multiplied by a linear function of ω to allow for spectral-weight redistribution between the coherent- and incoherent parts. Thus, $\chi_{s,\text{in}}''(\mathbf{k}, \omega) \equiv [B(\mathbf{k}) + \omega C(\mathbf{k})] \cdot \chi_{s,\text{L}}''(\mathbf{k}, \omega)$, where $B(\mathbf{k}) \geq 0$ and $C(\mathbf{k})$ are free \mathbf{k} -dependent parameters. This form of $\chi_{s,\text{in}}''(\mathbf{k}, \omega)$ reflects the fermiology of the underlying correlated electronic system.

Results—Representative least-squares fits of imaginary parts of the SGA $_f$ +1/ \mathcal{N}_f susceptibilities over the energy range approximately encompassing non-zero values of $\chi_s''(\mathbf{k}, \omega)$, are displayed in left panels of Fig. 2.

Blue circles in (a), (c), (e) and (g) represent calculated $\chi_s''(\mathbf{k}, \omega)$ for $\mathbf{k} = (0.5, 0, 0)$, $(0.5, 0.5, 0)$, $(0.03, 0, 0)$, and $(0.03, 0.03, 0)$, respectively. The green and blue regions are the incoherent and harmonic parts, respectively. The red line marks sum of the two, reproducing faithfully the SGA $_f$ +1/ \mathcal{N}_f result. For completeness, by black dotted lines we depict the Lindhard susceptibility, character of which varies across the BZ. A substantial directional anisotropy of spin dynamics is apparent, with coherent oscillator peaks appearing only along the anti-nodal line. In the right panels, the corresponding charge response, $\chi_c''(\mathbf{k}, \omega)$, is plotted. A clear distinction between the incoherent part and plasmon peak should be noted for the experimentally relevant regime of small in-plane momentum transfers, hence we identify the plasmon energy with the peak position in $\chi_c''(\mathbf{k}, \omega)$.

We now proceed to a unified quantitative analysis of both paramagnon and plasmon dynamics in $(\text{Bi, Pb})_2(\text{Sr, La})_2\text{CuO}_{6+\delta}$. In Fig. 3 we compare the calculated SGA $_f$ +1/ \mathcal{N}_f paramagnon characteristics with RIXS data for hole-doping levels $\delta = 0.21$ [(a), (d), (g)], $\delta = 0.16$ [(b), (e), (h)], and $\delta = 0.11$ [(c), (f), (i)]. Top panels [(a)-(c)] show the SGA $_f$ +1/ \mathcal{N}_f (red solid lines) and RIXS [19] (solid circles) paramagnon propagation energies, $\omega_p(\mathbf{k})$. Color maps represent imaginary part of the dynamical spin susceptibility, with blue and white colors mapping to low- and high-intensity regions, respectively. The agreement between theory and experiment is semi-quantitative for all doping levels, with the exception of the Γ - M direction for $\delta = 0.11$. In the latter case, SGA $_f$ +1/ \mathcal{N}_f yields overdamped magnetic dynamics ($\omega_p(\mathbf{k}) = 0$), whereas RIXS data corresponds to substantially damped, but still resonant response. A significant anisotropy between the nodal (Γ - M) and anti-nodal (Γ - X) directions is consistently observed both in SGA $_f$ +1/ \mathcal{N}_f and experimental data. Namely, the anti-nodal paramagnons persist across the entire doping range, but become rapidly overdamped with increasing doping along the nodal line. We note that a comparable agreement with RIXS paramagnon spectra has been recently achieved within a single-layer model [39]. This points towards a predominately two-dimensional character of spin excitations, which is also supported by investigation of the static response, detailed below.

In Fig. 3(d)-(f) and 3(g)-(i), we carry out an analysis of the underlying bare paramagnon energies and damping, $\omega_0(\mathbf{k})$ and $\gamma(\mathbf{k})$, respectively. Solid lines mark the parameters extracted from SGA $_f$ +1/ \mathcal{N}_f spin susceptibilities, with the use of model (3), whereas solid circles are RIXS data of Ref. [19], processed in an analogous manner. The overall agreement of both quantities with experiment is semi-quantitative across the phase diagram, with the exception of the Γ - M line in the underdoped case, where SGA $_f$ +1/ \mathcal{N}_f yields larger damping rates, and close to the Γ point for the overdoped situation.

We turn next to the discussion of charge excitations

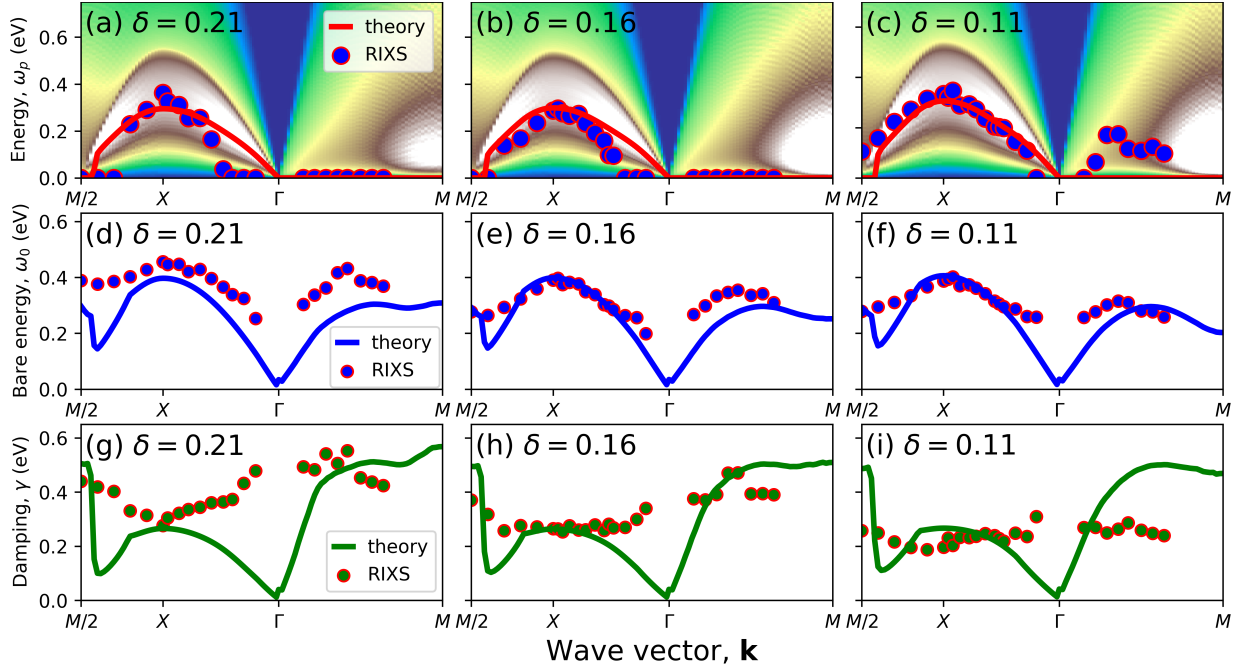


FIG. 3. Paramagnon energies for $(\text{Bi, Pb})_2(\text{Sr, La})_2\text{CuO}_{6+\delta}$ along the $M/2\text{-}X\text{-}\Gamma\text{-}M$ Brillouin-zone contour. To panels [(a)-(c)] show the propagation energy, ω_p , as obtained from $\text{SGA}_f+1/\mathcal{N}_f$ approach (red solid lines) and experiment[19] (circles) at three hole-doping levels, $\delta = 0.21$, $\delta = 0.16$, and $\delta = 0.11$. The color maps represent calculated imaginary part of dynamical spin susceptibility, ranging from blue (low intensity) to white (high intensity). Panels (d)-(f) and (g)-(i) show the bare paramagnon energies and damping rate (ω_0 and γ , respectively). Lines and circles are $\text{SGA}_f+1/\mathcal{N}_f$ results and RIXS data [19], respectively.

for the same model parameters as those used to generate Fig. 3. The wave-vector transfers are hereafter represented as $\mathbf{k} = (h\frac{2\pi}{a}, 0, l\frac{2\pi}{c})$, with c taken as $2d$ to account for two primitive cells in a crystallographic cell [53]. In Fig. 4(a), the calculated plasmon energies as a function of l are displayed for $h = 0.03$ (blue line) and $h = 0.05$ (red line), and compared with the corresponding RIXS data [25] for $\text{Bi}_2\text{Sr}_{1.6}\text{La}_{0.4}\text{CuO}_{6+\delta}$. For reference, in panel (b) we show raw imaginary part of the $\text{SGA}_{\lambda_d}+1/\mathcal{N}_f$ charge susceptibility for $h = 0.03$, used to obtain theoretical dispersion curve [blue line in (a)]. Panel (c) exhibits in-plane plasmon dispersion relations for two fixed values of the out-of-plane wave-vector transfer, $l = 1.5$ and $l = 1.75$, as a function of h . In panel (d), we display unprocessed χ''_c for $l = 1.5$. The agreement between theory and experiment is quantitative along all BZ contours. As is seen in Fig. 4(a), plasmon modes disperse strongly along the out-of-plane direction, with the minimum energy for $l = 1$, corresponding to anti-phase charge fluctuations on neighboring CuO_2 planes.

For the sake of completeness, we also examine stability of the paramagnetic metallic state against fluctuations. In Fig. 5, static spin [panel (a)] and charge [panel (b)] susceptibilities are displayed along the $\Gamma\text{-}X\text{-}M\text{-}\Gamma\text{-}Z\text{-}R\text{-}A\text{-}Z$ contour (cf. Fig. 1) for the three doping levels, $\delta = 0.21$, 0.16 , and 0.11 . The susceptibilities remain finite along the high-symmetry directions, with an increasing tendency towards antiferromagnetic instability as half-filling

is approached [enhanced values of $\chi'_s(\mathbf{k}, \omega = 0)$ at the M point; cf. panel (a)]. On the other hand, the charge response [panel (b)] depends only weakly on doping, indicating that the system stays clear of charge-density-wave (CDW) order in the considered temperature range. As is seen in Fig. 5, spin fluctuations are two-dimensional with barely distinguishable $\Gamma\text{-}X\text{-}M\text{-}\Gamma$ and $Z\text{-}R\text{-}A\text{-}Z$ profiles, whereas charge response exhibits qualitatively distinct behavior around Γ and Z points. Our results support the physical picture of at most moderate screening of the non-local Coulomb interaction, so that the plasmon excitations are influenced by its algebraic tail. On the other hand, the paramagnons are weakly affected by the non-local terms. The three-dimensional extension of the Hubbard model with inclusion of the long-range interactions is thus required primarily to quantitatively describe charge excitations. The impact of those terms on equilibrium properties has been discussed elsewhere [45].

Outlook—We have carried out a quantitative analysis of collective spin- and charge excitations in a microscopic model of high- T_c copper-oxides. Those modes are present in wide temperature and doping range and, in particular, in the regime where no long-range spin-density-wave or CDW order occur. The principal difficulty in describing them is due to the strongly-correlated character of the underlying electronic states. This circumstance necessitates a generalization of Moriya-Hertz-Millis-type approach to incorporate fluctuations into a

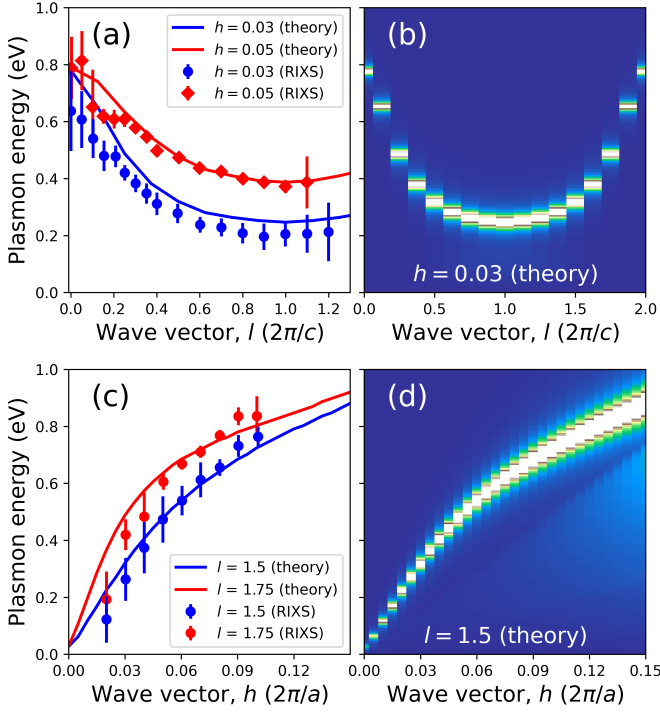


FIG. 4. Plasmon dispersion in $\text{Bi}_2\text{Sr}_{1.6}\text{La}_{0.4}\text{CuO}_{6+\delta}$ at doping $\delta = 0.16$. Lines and symbols are $\text{SGAF}+1/\mathcal{N}_f$ results and the RIXS data of Ref. [25], respectively. Panel (a) shows the data as a function the out-of-plane momentum transfer, l , for fixed $h = 0.03$ (blue color) and $h = 0.05$ (red color). In panel (c), two in-plane cuts for $l = 1.5$ (blue) and $l = 1.75$ (red) are displayed. In (b) and (d), the corresponding raw $\text{SGAF}+1/\mathcal{N}_f$ dynamical charge susceptibilities are shown. Wave vectors are expressed as $\mathbf{k} = (h\frac{2\pi}{a}, 0, l\frac{2\pi}{c})$, with $c = 2d$.

nonstandard reference state and going systematically beyond the renormalized mean-field theory (RMFT) [40]. The dynamical effects are included by $1/\mathcal{N}_f$ expansion around the variationally-determined saddle-point solution, reproducing the experimental data semi-quantitatively within a single scheme and for once fixed microscopic parameters [cf. Figs. 3(a-c) and 4(a-b)]. In conjunction with the former comprehensive VWF analysis of the static- and single-particle properties of high- T_c cuprates [30, 41–45], encompassing SC/CDW phases, Fermi-velocity/wave-vector, quasiparticle masses, and kinetic energy gain at SC transition, we arrive here at a consistent semi-quantitative description of both static- and collective dynamic properties of hole-doped high- T_c materials. Those aspects should be studied further within a more realistic three-band model of high- T_c SC, either in the Hubbard or t - J - U - V form [30].

The untouched here questions comprise pseudogap formation and temperature-dependence of electrical resistivity, when the quantum fluctuations are tackled explicitly along the lines presented here. This requires supplementing the present approach with calculations of single-particle self-energy and subleading fluctuation

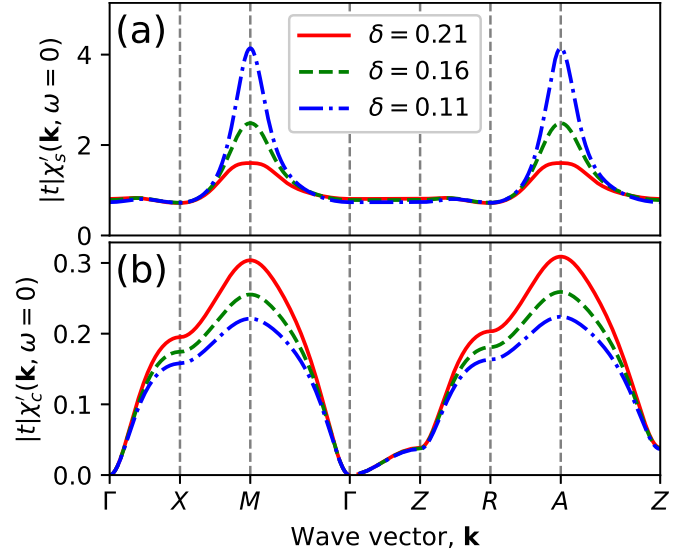


FIG. 5. Calculated static spin [panel (a)] and charge [panel (b)] susceptibilities for hole doping $\delta = 0.21$ (red solid lines), $\delta = 0.16$ (green dashed line), and $\delta = 0.11$ (blue dash-dotted line). The universal feature at point M [in the case (a)] and at Γ [in the case (b)] should be noted.

free-energy corrections, all in a fully self-consistent manner. Such a task poses a substantial challenge. Finally, within the *strong-correlation picture*, both the real-space pairing and AF correlations in the cuprates share the same source: kinetic exchange interaction $\propto \hat{\mathbf{S}}_i \hat{\mathbf{S}}_j - \frac{1}{4} \hat{n}_i \hat{n}_j$, that may be equivalently expressed in terms of singlet pairing operators $\hat{b}_{ij}^\dagger \equiv \frac{1}{\sqrt{2}}(\hat{c}_{i\uparrow}^\dagger \hat{c}_{j\downarrow}^\dagger - \hat{c}_{i\downarrow}^\dagger \hat{c}_{j\uparrow}^\dagger)$ [54]. The considered here paramagnetic ground state is also spin singlet, and the elementary paramagnon excitations are associated with singlet-triplet ($S = 0$ to $S = 1$) transitions. Their robustness in hole-doped cuprates supports thus indirectly also the exchange-driven real-space pairing viewpoint, calling for an extension of the VWF+ $1/\mathcal{N}_f$ approach to incorporate the SC state. This requires accounting for the SC gap fluctuations through the anomalous lines, $S_{i\sigma j\sigma'} = \langle \hat{c}_{i\sigma} \hat{c}_{j\sigma'} \rangle$ [30, 43, 55], introducing additional complexity to the problem, and should be treated separately.

To recapitulate, the VWF solution going systematically beyond RMFT (DE-GWF scheme [30, 41–45]), combined with the present VWF+ $1/\mathcal{N}_f$ approach, supports in a quantitative manner a mutual relationship between strong-electronic correlations and collective dynamics in high- T_c cuprates.

Acknowledgments—This work was supported by Grant OPUS No. UMO-2018/29/B/ST3/02646 from Narodowe Centrum Nauki and by a grant from the SciMat Priority Research Area under the Strategic Programme Excellence Initiative at the Jagiellonian University.

* maciej.fidrysiak@uj.edu.pl

† jozef.spalek@uj.edu.pl

- [1] B. Keimer, S. A. Kivelson, M. R. Norman, S. Uchida, and J. Zaanen, "From quantum matter to high-temperature superconductivity in copper oxides," *Nature* **518**, 179 (2015).
- [2] R. Coldea, S. M. Hayden, G. Aeppli, T. G. Perring, C. D. Frost, T. E. Mason, S.-W. Cheong, and Z. Fisk, "Spin Waves and Electronic Interactions in La_2CuO_4 ," *Phys. Rev. Lett.* **86**, 5377 (2001).
- [3] Y. Y. Peng, G. Dellea, M. Minola, M. Conni, A. Amorese, D. Di Castro, G. M. De Luca, K. Kummer, M. Salluzzo, X. Sun, X. J. Zhou, G. Balestrino, M. Le Tacon, B. Keimer, L. Braicovich, N. B. Brookes, and G. Ghiringhelli, "Influence of apical oxygen on the extent of in-plane exchange interaction in cuprate superconductors," *Nat. Phys.* **13**, 1201 (2017).
- [4] M. P. M. Dean, G. Dellea, R. S. Springell, F. Yakhov-Harris, K. Kummer, N. B. Brookes, X. Liu, Y.-J. Sun, J. Strle, T. Schmitt, L. Braicovich, G. Ghiringhelli, I. Božović, and J. P. Hill, "Persistence of magnetic excitations in $\text{La}_{2-x}\text{Sr}_x\text{CuO}_4$ from the undoped insulator to the heavily overdoped non-superconducting metal," *Nat. Mater.* **12**, 1019 (2013).
- [5] K. Ishii, M. Fujita, T. Sasaki, M. Minola, G. Dellea, C. Mazzoli, K. Kummer, G. Ghiringhelli, L. Braicovich, T. Tohyama, K. Tsutsumi, K. Sato, R. Kajimoto, K. Ikeuchi, K. Yamada, M. Yoshida, M. Kurooka, and J. Mizuki, "High-energy spin and charge excitations in electron-doped copper oxide superconductors," *Nat. Commun.* **5**, 3714 (2014).
- [6] W. S. Lee, J. J. Lee, E. A. Nowadnick, S. Gerber, W. Tabis, S. W. Huang, V. N. Strocov, E. M. Motoyama, G. Yu, B. Moritz, H. Y. Huang, R. P. Wang, Y. B. Huang, W. B. Wu, C. T. Chen, D. J. Huang, M. Greven, T. Schmitt, Z. X. Shen, and T. P. Devereaux, "Asymmetry of collective excitations in electron- and hole-doped cuprate superconductors," *Nat. Phys.* **10**, 883 (2014).
- [7] M. Guarise, B. Dalla Piazza, H. Berger, E. Gianini, T. Schmitt, H. M. Rønnow, G. A. Sawatzky, J. van den Brink, D. Altenfeld, I. Eremin, and M. Grioni, "Anisotropic softening of magnetic excitations along the nodal direction in superconducting cuprates," *Nat. Commun.* **5**, 5760 (2014).
- [8] S. Wakimoto, K. Ishii, H. Kimura, M. Fujita, G. Dellea, K. Kummer, L. Braicovich, G. Ghiringhelli, L. M. Debeer-Schmitt, and G. E. Granroth, "High-energy magnetic excitations in overdoped $\text{La}_{2-x}\text{Sr}_x\text{CuO}_4$ studied by neutron and resonant inelastic x -ray scattering," *Phys. Rev. B* **91** (2015).
- [9] M. Minola, Y. Lu, Y. Y. Peng, G. Dellea, H. Gretarsson, M. W. Haverkort, Y. Ding, X. Sun, X. J. Zhou, D. C. Peets, L. Chauviere, P. Dosanjh, D. A. Bonn, R. Liang, A. Damascelli, M. Dantz, X. Lu, T. Schmitt, L. Braicovich, G. Ghiringhelli, B. Keimer, and M. Le Tacon, "Crossover from Collective to Incoherent Spin Excitations in Superconducting Cuprates Probed by Detuned Resonant Inelastic X-Ray Scattering," *Phys. Rev. Lett.* **119**, 245133 (2017).
- [10] O. Ivashko, N. E. Shaik, X. Lu, C. G. Fatuzzo, M. Dantz, P. G. Freeman, D. E. McNally, D. Destraz, N. B. Christensen, T. Kurosawa, N. Momono, M. Oda, C. E. Matt, C. Monney, H. M. Rønnow, T. Schmitt, and J. Chang, "Damped spin excitations in a doped cuprate superconductor with orbital hybridization," *Phys. Rev. B* **95** (2017).
- [11] D. Meyers, H. Miao, A. C. Walters, V. Bisogni, R. S. Springell, M. d'Astuto, M. Dantz, J. Pellicciari, H. Y. Huang, J. Okamoto, D. J. Huang, J. P. Hill, X. He, I. Božović, T. Schmitt, and M. P. M. Dean, "Doping dependence of the magnetic excitations in $\text{La}_{2-x}\text{Sr}_x\text{CuO}_4$," *Phys. Rev. B* **95**, 075139 (2017).
- [12] S. Gerber, X. Lu, C. Jia, Y. Huang, D. E. McNally, Y. Wang, F. H. Vernay, A. Keren, M. Shi, B. Moritz, Z.-X. Shen, T. Schmitt, T. P. Devereaux, L. Chaix, E. W. Huang, and W.-S. Lee, "Resonant inelastic x -ray scattering studies of magnons band bimagnons in the lightly doped cuprate $\text{La}_{2-x}\text{Sr}_x\text{CuO}_4$," *Phys. Rev. B* **97**, 155144 (2018).
- [13] H. C. Robarts, M. Barthélemy, K. Kummer, M. García-Fernández, J. Li, A. Nag, A. C. Walters, K. J. Zhou, and S. M. Hayden, "Anisotropic damping and wave vector dependent susceptibility of the spin fluctuations in $\text{La}_{2-x}\text{Sr}_x\text{CuO}_4$ studied by resonant inelastic x -ray scattering," *Phys. Rev. B* **100**, 214510 (2019).
- [14] K.-J. Zhou, Y.-B. Huang, C. Monney, X. Dai, V. N. Strocov, N.-L. Wang, Z.-G. Chen, C. Zhang, P. Dai, L. Patthey, J. van den Brink, H. Ding, and T. Schmitt, "Persistent high-energy spin excitations in iron-pnictide superconductors," *Nat. Commun.* **4**, 1470 (2013).
- [15] H. Gretarsson, N. H. Sung, J. Porras, J. Bertinshaw, C. Dietl, Jan A. N. Bruin, A. F. Bangura, Y. K. Kim, R. Dinnebier, Jungho Kim, A. Al-Zein, M. Moretti Sala, M. Krisch, M. Le Tacon, B. Keimer, and B. J. Kim, "Persistent Paramagnons Deep in the Metallic Phase of $\text{Sr}_{2-x}\text{La}_x\text{IrO}_4$," *Phys. Rev. Lett.* **117**, 107001 (2016).
- [16] R. Fumagalli, L. Braicovich, M. Minola, Y. Y. Peng, K. Kummer, D. Betto, M. Rossi, E. Lefrançois, C. Morawe, M. Salluzzo, H. Suzuki, F. Yakhov, M. Le Tacon, B. Keimer, N. B. Brookes, M. Moretti Sala, and G. Ghiringhelli, "Polarization-resolved Cu L_3 -edge resonant inelastic x -ray scattering of orbital and spin excitations in $\text{NdBa}_2\text{Cu}_3\text{O}_{7-\delta}$," *Phys. Rev. B* **99**, 134517 (2019).
- [17] M. Le Tacon, G. Ghiringhelli, J. Chaloupka, M. Moretti Sala, V. Hinkov, M. W. Haverkort, M. Minola, M. Bakr, K. J. Zhou, S. Blanco-Canosa, C. Monney, Y. T. Song, G. L. Sun, C. T. Lin, G. M. De Luca, M. Salluzzo, G. Khaliullin, T. Schmitt, L. Braicovich, and B. Keimer, "Intense paramagnon excitations in a large family of high-temperature superconductors," *Nat. Phys.* **7**, 725 (2011).
- [18] C. J. Jia, E. A. Nowadnick, K. Wohlfeld, Y. F. Kung, C.-C. Chen, S. Johnston, T. Tohyama, B. Moritz, and T. P. Devereaux, "Persistent spin excitations in doped antiferromagnets revealed by resonant inelastic light scattering," *Nat. Commun.* **5**, 3314 (2014).
- [19] Y. Y. Peng, E. W. Huang, R. Fumagalli, M. Minola, Y. Wang, X. Sun, Y. Ding, K. Kummer, X. J. Zhou, N. B. Brookes, B. Moritz, L. Braicovich, T. P. Devereaux, and G. Ghiringhelli, "Dispersion, damping, and intensity of spin excitations in the monolayer $(\text{Bi,Pb})_2(\text{Sr,L a})_2\text{CuO}_{6+\delta}$ cuprate superconductor family," *Phys. Rev. B* **98** (2018).
- [20] K. Ishii, T. Tohyama, S. Asano, K. Sato, M. Fujita, S. Wakimoto, K. Tustsui, S. Sota, J. Miyawaki, H. Niwa, Y. Harada, J. Pellicciari, Y. Huang, T. Schmitt, Y. Ya-

- mamoto, and J. Mizuki, “Observation of momentum-dependent charge excitations in hole-doped cuprates using resonant inelastic x -ray scattering at the oxygen K edge,” *Phys. Rev. B* **96**, 115148 (2017).
- [21] M. Hepting, L. Chaix, E. W. Huang, R. Fumagalli, Y. Y. Peng, B. Moritz, K. Kummer, N. B. Brookes, W. C. Lee, M. Hashimoto, T. Sarkar, J.-F. He, C. R. Rotundu, Y. S. Lee, R. L. Greene, L. Braicovich, G. Ghiringhelli, Z. X. Shen, T. P. Devereaux, and W. S. Lee, “Three-dimensional collective charge excitations in electron-doped copper oxide superconductors,” *Nature* **563**, 374 (2018).
- [22] K. Ishii, M. Kurooka, Y. Shimizu, M. Fujita, K. Yamada, and J. Mizuki, “Charge Excitations in $\text{Nd}_{2-x}\text{Ce}_x\text{CuO}_4$ Observed with Resonant Inelastic X -ray Scattering: Comparison of Cu K -edge with Cu L_3 -edge,” *J. Phys. Soc. Japan* **88**, 075001 (2019).
- [23] J. Lin, J. Yuan, K. Jin, Z. Yin, Gang Li, K.-J. Zhou, X. Lu, M. Dantz, T. Schmitt, H. Ding, H. Guo, M. P. M. Dean, and X. Liu, “Doping evolution of the charge excitations and electron correlations in electron-doped superconducting $\text{La}_{2-x}\text{Ce}_x\text{CuO}_4$,” *npj Quant. Mater.* **5**, 4 (2020).
- [24] A. Singh, H. Y. Huang, Christopher Lane, J. H. Li, J. Okamoto, S. Komiyama, Robert S. Markiewicz, Arun Bansil, A. Fujimori, C. T. Chen, and D. J. Huang, “Acoustic plasmons and conducting carriers in hole-doped cuprate superconductors,” (2020), arXiv:2006.13424.
- [25] A. Nag, M. Zhu, M. Bejas, J. Li, H. C. Robarts, H. Yamase, A. N. Petsch, D. Song, H. Eisaki, A. C. Walters, M. García-Fernández, A. Greco, S. M. Hayden, and K.-J. Zhou, “Detection of Acoustic Plasmons in Hole-Doped Lanthanum and Bismuth Cuprate Superconductors Using Resonant Inelastic X -Ray Scattering,” *Phys. Rev. Lett.* **125**, 257002 (2020).
- [26] S. Wakimoto, H. Zhang, K. Yamada, I. Swainson, Hyunkyung Kim, and R. J. Birgeneau, “Direct Relation between the Low-Energy Spin Excitations and Superconductivity of Overdoped High- T_c Superconductors,” *Phys. Rev. Lett.* **92**, 217004 (2004).
- [27] T. Dahm, V. Hinkov, S. V. Borisenko, A. A. Kordyuk, V. B. Zabolotnyy, J. Fink, B. Büchner, D. J. Scalapino, W. Hanke, and B. Keimer, “Strength of the spin-fluctuation-mediated pairing interaction in a high-temperature superconductor,” *Nat. Phys.* **5**, 217 (2009).
- [28] M. Grilli, R. Raimondi, C. Castellani, C. Di Castro, and G. Kotliar, “Superconductivity, phase separation, and charge-transfer instability in the $U=\infty$ limit of the three-band model of the CuO_2 planes,” *Phys. Rev. Lett.* **67**, 259 (1991).
- [29] A. Perali, C. Castellani, C. Di Castro, and M. Grilli, “ d -wave superconductivity near charge instabilities,” *Phys. Rev. B* **54**, 16216 (1996).
- [30] J. Spałek, M. Zegrodnik, and J. Kaczmarczyk, “Universal properties of high-temperature superconductors from real-space pairing: t - J - U model and its quantitative comparison with experiment,” *Phys. Rev. B* **95**, 024506 (2017).
- [31] A. Greco, H. Yamase, and M. Bejas, “Plasmon excitations in layered high- T_c cuprates,” *Phys. Rev. B* **94**, 075139 (2016).
- [32] A. Greco, H. Yamase, and M. Bejas, “Charge-Density-Excitation Spectrum in the t - t' - J - V Model,” *J. Phys. Soc. Japan* **86**, 034706 (2017).
- [33] A. Greco, H. Yamase, and M. Bejas, “Close inspection of plasmon excitations in cuprate superconductors,” *Phys. Rev. B* **102**, 024509 (2020).
- [34] R. S. Markiewicz, M. Z. Hasan, and A. Bansil, “Acoustic plasmons and doping evolution of Mott physics in resonant inelastic x -ray scattering from cuprate superconductors,” *Phys. Rev. B* **77**, 094518 (2008).
- [35] A. Greco, H. Yamase, and M. Bejas, “Origin of high-energy charge excitations observed by resonant inelastic X -ray scattering in cuprate superconductors,” *Commun. Phys.* **2**, 3 (2019).
- [36] A. Foussats and A. Greco, “Large- N expansion based on the Hubbard operator path integral representation and its application to the t - J model,” *Phys. Rev. B* **65**, 195107 (2002).
- [37] A. Foussats and A. Greco, “Large- N expansion based on the Hubbard operator path integral representation and its application to the t - J model. II. The case for finite J ,” *Phys. Rev. B* **70**, 205123 (2004).
- [38] H.-Y. Zhang, X.-Q. Wu, F.-J. Kong, Y.-J. Bai, and N. Xu, “Doping evolution of the magnetic excitations in the monolayer CuO_2 ,” *J. Phys.: Condens. Matter* **32**, 415603 (2020).
- [39] M. Fidrysiak and J. Spałek, “Robust spin and charge excitations throughout the high- T_c cuprate phase diagram from incipient Mottness,” *Phys. Rev. B* **102**, 014505 (2020).
- [40] M. Fidrysiak and J. Spałek, “Universal collective modes from strong electronic correlations: Modified $1/N_f$ theory with application to high- T_c cuprates,” *Phys. Rev. B* **103**, 165111 (2021).
- [41] M. Zegrodnik and J. Spałek, “Universal properties of high-temperature superconductors from real-space pairing: Role of correlated hopping and intersite Coulomb interaction within the t - J - U model,” *Phys. Rev. B* **96**, 054511 (2017).
- [42] M. Zegrodnik and J. Spałek, “Effect of interlayer processes on the superconducting state within the t - J - U model: Full Gutzwiller wave-function solution and relation to experiment,” *Phys. Rev. B* **95**, 024507 (2017).
- [43] M. Fidrysiak, M. Zegrodnik, and J. Spałek, “Realistic estimates of superconducting properties for the cuprates: reciprocal-space diagrammatic expansion combined with variational approach,” *J. Phys.: Condens. Matter* **30**, 475602 (2018).
- [44] M. Zegrodnik and J. Spałek, “Incorporation of charge- and pair-density-wave states into the one-band model of d -wave superconductivity,” *Phys. Rev. B* **98**, 155144 (2018).
- [45] M. Zegrodnik, A. Biborski, M. Fidrysiak, and J. Spałek, “Superconductivity in the three-band model of cuprates: nodal direction characteristics and influence of intersite interactions,” (2020), *J. Phys.: Condens. Matter* (in press), arXiv:2009.04922.
- [46] F. Nilsson, K. Karlsson, and F. Aryasetiawan, “Dynamically screened Coulomb interaction in the parent compounds of hole-doped cuprates: Trends and exceptions,” *Phys. Rev. B* **99**, 075135 (2019).
- [47] F. Becca, M. Tarquini, M. Grilli, and C. Di Castro, “Charge-density waves and superconductivity as an alternative to phase separation in the infinite- U Hubbard-Holstein model,” *Phys. Rev. B* **54**, 12443 (1996).
- [48] E. van Heumen, W. Meevasana, A. B. Kuzmenko,

- H. Eisaki, and D. van der Marel, “Doping-dependent optical properties of Bi2201,” *New J. Phys.* **11**, 055067 (2009).
- [49] M. Hirayama, Y. Yamaji, T. Misawa, and M. Imada, “Ab initio effective Hamiltonians for cuprate superconductors,” *Phys. Rev. B* **98**, 134501 (2018).
- [50] P. A. Igoshev, M. A. Timirgazin, V. F. Gilmutdinov, A. K. Arzhnikov, and V. Yu Irkhin, “Spiral magnetism in the single-band Hubbard model: the Hartree-Fock and slave-boson approaches,” *J. Phys.: Condens. Matter* **27**, 446002 (2015).
- [51] J. Jędrak and J. Spałek, “Renormalized mean-field t - J model of high- T_c superconductivity: Comparison to experiment,” *Phys. Rev. B* **83**, 104512 (2011).
- [52] J. Lamsal and W. Montfrooij, “Extracting paramagnon excitations from resonant inelastic x -ray scattering experiments,” *Phys. Rev. B* **93**, 214513 (2016).
- [53] N. N. Kovaleva, A. V. Boris, T. Holden, C. Ulrich, B. Liang, C. T. Lin, B. Keimer, C. Bernhard, J. L. Tallon, D. Munzar, and A. M. Stoneham, “ c -axis lattice dynamics in Bi-based cuprate superconductors,” *Phys. Rev. B* **69**, 054511 (2004).
- [54] J. Spałek, “Effect of pair hopping and magnitude of intratomic interaction on exchange-mediated superconductivity,” *Phys. Rev. B* **37**, 533 (1988).
- [55] M. Abram, M. Zegrodnik, and J. Spałek, “Antiferromagnetism, charge density wave, and d-wave superconductivity in the extended t - J - U model: role of intersite Coulomb interaction and a critical overview of renormalized mean field theory,” *J. Phys.: Condens. Matter* **29**, 365602 (2017).